Embedding atomic cobalt into graphene lattices to active room-temperature ferromagnetism

Wei Hu
University of Science and Technology of China
Chao Wang
University of Science and Technology of China
Hao Tan
University of Science and Technology of China
Hengli Duan
University of Science and Technology of China
Guinan Li
University of Science and Technology of China
Na Li
University of Science and Technology of China
Qianqian Ji
University of Science and Technology of China
Ying Lu
University of Science and Technology of China
Yao Wang
University of Science and Technology of China
Zhihu Sun
University of Science and Technology of China https://orcid.org/0000-0002-3898-969X
Fengchun Hu
University of Science & Technology of China
Wensheng Yan (ywsh2000@ustc.edu.cn)
University of Science and Technology of China https://orcid.org/0000-0001-6297-4589

Article

Keywords: Room temperature ferromagnetism, square-planar Co-N4 moieties, d-p orbital hybridization, Stoner ferromagnetism, graphene based spintronics

Posted Date: July 30th, 2020

DOI: https://doi.org/10.21203/rs.3.rs-45823/v1

Version of Record: A version of this preprint was published at Nature Communications on March 25th, 2021. See the published version at https://doi.org/10.1038/s41467-021-22122-2.

Embedding atomic cobalt into graphene lattices to active room-temperature ferromagnetism

Wei Hu,[1] Chao Wang,[*,1] Hao Tan,[1] Hengli Duan,[1] Guinan Li,[1] Na Li,[1] Qianqian Ji,[1] Ying Lu,[1] Yao Wang,[1] Zhihu Sun,[*,1] Fengchun Hu,[1] and Wensheng Yan[*,1]

[1]National Synchrotron Radiation Laboratory, University of Science and Technology of China, Hefei 230029, P. R. China

Abstract: Graphene is extremely promising for next-generation spintronics applications; however, realizing graphene-based room-temperature magnets remains a great challenge. Here, for the first time, we demonstrate that robust room-temperature ferromagnetism with T_C up to ~400 K and saturation magnetization of 0.11 emu/g (300 K) can be achieved in graphene by embedding isolated Co atoms with the aid of coordinated N atoms. Extensive structural characterizations show that square-planar Co-N_4 moieties were formed in the graphene lattices, where atomically dispersed Co atoms provide local magnetic moments. Detailed electronic structure calculations reveal that the *d-p* orbital hybridization between the embedded Co and matrix N/C atoms generates spin polarization for the delocalized N/C $2p_z$ electrons and consequently enhances the long-range coupling through Stoner ferromagnetism. This work provides an effective means to induce room-temperature ferromagnetism in graphene and may open the possibilities for developing graphene-based spintronics devices.

Keywords: Room-temperature ferromagnetism; square-planar Co-N_4 moieties; *d-p* orbital hybridization; Stoner ferromagnetism; graphene-based spintronics

Introduction

Graphene is a two-dimensional (2D) layered material composed of one-atom-thickness hexagonal networks of sp^2-hybridized carbon.[1,2] It possesses many unique properties such as large specific surface area,[3] superior mechanical strength,[4] high intrinsic carrier mobility[5,6] and thermal conductivity.[7] Great efforts have been devoted to promoting the applications of graphene in a diversity of fields including field-effect transistors,[8] chemical sensors,[9] fuel cells,[10] and so forth. Graphene is also envisaged to be a highly promising material for next-generation spintronic applications, owing to its extraordinary carrier mobility, long spin diffusion length, weak intrinsic spin-orbit coupling and limited hyperfine interactions.[11,12] For practical applications in spintronic devices, the graphene-based material is required to be ferromagnetic above room temperature. Unfortunately, the pristine graphene is intrinsically diamagnetic and lacks local magnetic moments.[13,14] Therefore, development of effective strategies to induce and manipulate the ferromagnetism of graphene has become a key issue to extend its applications in spintronics.

So far, various strategies have been attempted to realize ferromagnetic ordering in graphene, including utilization of atomic vacancies,[15] sp^3 functionlization,[16] chemical doping,[14,17] surface adsorption[18] and zigzag edges.[19] However, the magnetic moments induced by point defects or edges are relatively weak and unstable; and consequently the ferromagnetic ordering often collapses at rather low temperatures.[14,16,17,20,21] For instance, Grigorieva et al. produced high-density vacancy defects on graphene with ion beam radiation and realized a macroscopic magnetic moment of 0.001 μ_B/atom; but no ferromagnetic coupling was observed at temperatures as low as liquid helium (4.2 K).[21] Tucek et al. found that S-doped graphene could only maintain ferromagnetic ordering at temperatures below 62 K,[14] and Liu et al. demonstrated that only pure diamagnetism can be observed in N-doped graphene at 300 K.[22] To improve the stability of ferromagnetic coupling, the common wisdom is to increase the content of defects so as to shorten the distance between weak local magnetic moments. However, too high content of defects would break the π-bonding networks and degrade the electric properties of graphene. In analogous 2D system of graphene like transition metal (TM)

dichalcogenides, doping of magnetic TM (Fe, Co, and Ni) has been experimentally demonstrated to be an effective method for inducing stable room-temperature ferromagnetic ordering.[23,24] However, direct doping of TM atoms in graphene is impracticable because graphene is not ionic crystal like TM dichalcogenides and its honeycomb networks are maintained by strong C-C covalent bonds. This makes the energy barrier of embedding a single TM atom into pristine graphene lattices very steep. Indeed, previous attempts to produce TM-graphene compositions merely yielded TM atoms or clusters adsorbed on the surface of graphene,[25,26] where the magnetism is not intrinsic but mainly contributed by metal clusters. Meanwhile the adsorbed TM atoms on graphene could be easily dissociated or coagulated at elevated temperatures. For example, graphene with Co atoms attached on the surface can maintain ferromagnetic ordering only below 10 K.[26] Hence, stable anchoring of magnetic TM atoms on graphene is important for the manufacture of graphene-based room-temperature ferromagnetic materials. Inspired by the metal-nitrogen (M-N) moiety strategies developed recently for atomically dispersed TM catalysts,[27,28] we speculate that doping TM with the aid of coordinated N might be a possible way to embed TM atoms into graphene lattices. As the Pauling electronegativity of N (3.0) is significantly higher than that of C (2.5), the TM atoms can be strongly bound by N atoms rather than by C atoms as observed in many TM-N-C systems.[28,29] Therefore, the TM-N_x moiety can be doped in graphene and act as the ferromagnetic centers. Besides, previous density functional theory (DFT) simulations confirmed the structural stability of the heavy N-doped graphene at up to 1000 K,[30] further supporting the feasibility of TM-N_x moiety on building the graphene-based room-temperature ferromagnetic materials.

Herein, motivated by the above consideration, we propose a coordination atom assisted strategy by embedding magnetic TM into graphene lattices under the assistance of coordinated N atoms, where stable room-temperature ferromagnetism can be achieved in graphene. This strategy is exemplified by the single-metal-atomic Co-N_4 moiety doped graphene, which was synthesized via impregnation-pyrolysis method, and exhibits unprecedented ferromagnetic orderings with Curie temperature (T_C) up to ~400 K. A high saturation magnetization of 0.11 emu/g at 300 K (0.73 emu/g at 5 K) is

obtained at the Co content of 0.4 at. %. Detailed X-ray absorption spectroscopy characterization and multiple-scattering simulations confirm the embedding of Co atoms in the graphene lattices, via the formation of isolated Co-N_4 units. Electronic structure calculations reveal that stable room-temperature ferromagnetism arises from the Stoner mechanism induced by the *d-p* orbital hybridization between the embedded Co and C/N atoms. Moreover the *d-p* hybridization induced by the Co-N bonds could generate spin polarization for the delocalized N 2*p* and C 2*p* electrons, and consequently favor the long-range ferromagnetic coupling. Besides the ferromagnetic ordering, the Co-N_4 doped graphene possesses unique electronic structure where only one spin channel crosses the Fermi level, greatly benefiting the generation of spin-polarized current in spintronics.[31] This deliberately designed strategy opens up an avenue for the development of graphene-based spintronic devices.

Results

Analysis of sample morphology and structure. The atomically dispersed Co embedded N-doped graphene (named Co-N/G) was prepared through a two-step synthesis strategy consisting of the impregnation and following pyrolysis procedures. For comparison, samples with other Co contents were prepared, denoted as 0.2Co-N/G, 0.5Co-N/G, and 3Co-N/G with 0.2×, 0.5× and 3× Co precursors during preparation (see experimental details in the section of Methods). According to the X-ray photoelectron spectroscopy (XPS) analysis (Table S1 in the Supporting Information), the final Co contents in 0.2Co-N/G, 0.5Co-N/G, Co-N/G and 3Co-N/G are 0.11, 0.22, 0.40, and 1.32 at. %, respectively. The transmission electron microscopy (TEM) images reveal transparent and corrugation sheets for all the samples (Figure 1a-c and Figure S1a), typical morphology features for mono- and few-layered graphene-based materials. However, particles with an average diameter of ~20 nm are observed on the 3Co-N/G nanosheets (Figure S1b), indicating the formation of the second phase; meanwhile no particles were observed in the samples with lower Co contents. Energy dispersive X-ray (EDX) spectroscopy and aberration corrected high-angle annular dark-field scanning transmission electron microscopy (HAADF-STEM) were used to further

characterize the morphology of Co-N/G nanosheets. The EDX images (Figure 1d) suggest the homogeneous distribution of C, N and Co elements over the nanosheets. And in the HAADF-STEM image (Figure 1e), a number of bright spots (some of them are highlighted by red circles for close observation) in single-atom size, corresponding to the isolated Co atoms, are well dispersed across the nanosheets. The crystalline phase of the Co-N/G nanosheets was studied with the X-ray diffraction (XRD) pattern, in which a broad peaks at about 26.3° (Figure S2) can be indexed to the (002) plane of hexagonal graphite.[32,33] No Co-related second phases were detected. Furthermore, Co K-edge X-ray absorption near edge structure (XANES) spectra (Figure 1f), Fourier-transformed (FT) k^3-weighted Co K-edge extended X-ray absorption fine structure

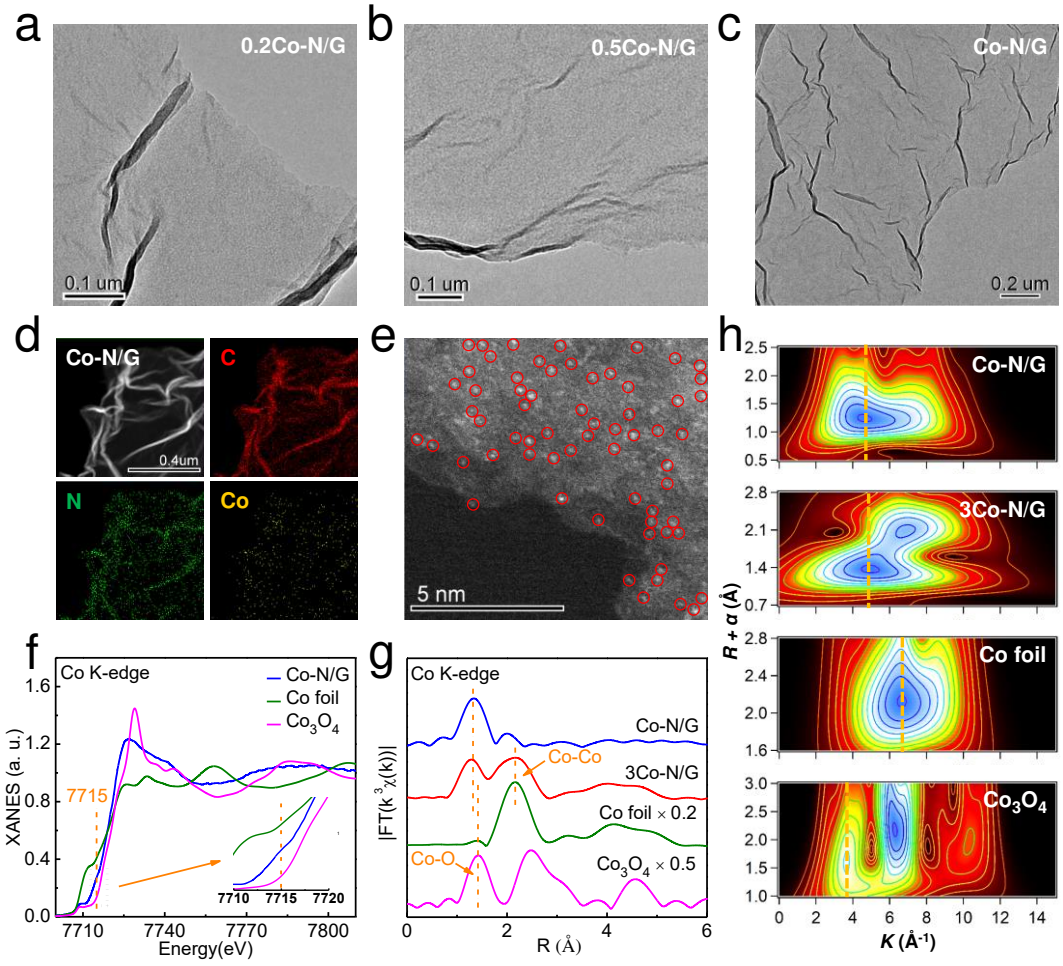

Figure 1. TEM images of a) 0.2Co-N/G, b) 0.5Co-N/G and c) Co-N/G samples. d) EDX elemental mapping and e) HAADF-STEM image of Co-N/G. f) Co K-edge XANES spectra for Co-N/G and reference samples. g) FT k^3-weighted Co K-edge EXAFS spectra and h) WT analysis of EXAFS spectra for Co-N/G, 3Co-N/G and reference samples.

(EXAFS) spectra (Figure 1g), and wavelet transform (WT) analysis (Figure 1h) also show that Co exists as isolated atoms in graphene (see details in Section II of the Supporting Information). All the above TEM and XAFS results confirm that atomically dispersed Co in Co-N/G nanosheets have been successfully synthesized, without the formation of Co-related second phase when the Co loading is below 0.4 at. %. When Co content is beyond 0.4 at. %, part of the Co atoms are in the form of metallic Co nanoparticles (Figures 1g and 1h, and Section II in the Supporting Information).

In order to explore the bonding configuration of Co atoms in Co-N/G nanosheets, X-ray photoelectron spectroscopy (XPS), N and C K-edge XANES measurements were performed. XPS survey spectrum (Figure S4) clearly shows the existence of C, N, and Co elements in Co-N/G nanosheets, while no other ferromagnetic impurities were detected. The corresponding fine-scan N 1*s* XPS spectrum of Co-N/G nanosheets shown in Figure 2a, can be deconvoluted into five component peaks. Besides the N 1*s* signal from of pyridinic (398.3 eV), pyrrolic (400.0 eV), graphitic (401.2 eV) and oxidized N groups (402.3 eV), there is also a signal from Co-N bonds with the XPS peak at ~399.2 eV.[32,34] The formation of Co-N bonds can be confirmed by N K-edge XANES spectra (Figure 2b), where an evident absorption peak B derived from Co-N bonding at ~399.5 eV can be observed, which is absent in the N/G nanosheets (see detailed N K-edge XANES analysis in Section III of the Supporting Information).[28,35] Further, the C K-edge XANES features of Co-N/G nanosheets (Figure 2c) are very similar to those of pristine graphene, indicating similar chemical environments of the carbon matrix, except for a feature at ~287.4 eV corresponding to the C-N bonding in

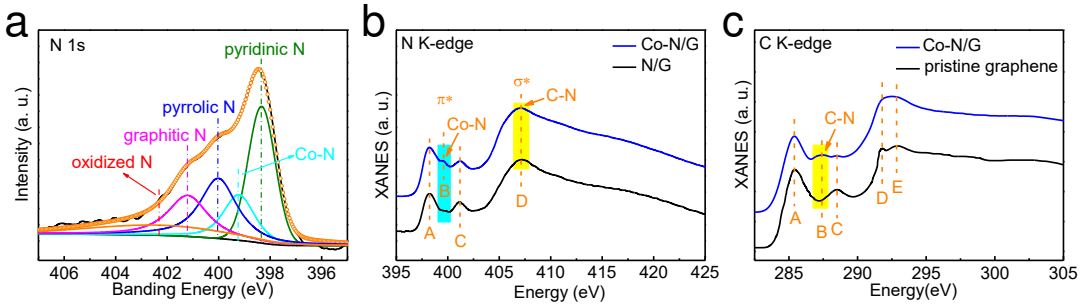

Figure 2. a) N 1*s* XPS spectrum of Co-N/G nanosheets. b) N K-edge XANES spectra of Co-N/G and N/G nanosheets. c) C K-edge XANES spectra of Co-N/G nanosheets and pristine graphene.

the C K-edge XANES of the Co-N/G nanosheets (see detailed C K-edge XANES analysis in Section IV of the Supporting Information).[36,37] Taking these analysis together, one can safely conclude that there is a specific Co-N-C structural moiety in Co-N/G nanosheets.

For quantitative analysis on the coordination configuration of Co atoms in Co-N/G nanosheets, a least-square EXAFS fitting was performed to extract the atomic structure parameters. Based on bonding configuration analysis, the best-fitting curves in *R*- and *q*-spaces for Co-N/G are shown in Figure 3a and Figure S5 by using Co-N backscattering path. The average coordination number of N atoms are estimated to be 4 with an average scattering distances of 1.95 Å (see details in Table S2 of the Supporting Information). It is worthy to note that, as displayed in Figure 1f, one pronounced pre-edge peak at about 7715 eV can be observed in the Co K-edge XANES spectrum for Co-N/G nanosheets. This is a typical feature of the $Co\text{-}N_4$ square-planar structure,[28,38] consistent with the EXAFS fitting results indicative of four N neighbors around a Co atom. The square-planar $Co\text{-}N_4$ configuration in Co-N/G could be further supported by the Co L_3-edge XANES spectrum as shown in Figure 3b, exhibits similar fine structure features (*a*, *b*, *c* and *d*) with those of cobalt pyrrolic (CoPc), but significantly different from those of Co metal and oxides as shown in Figure S6. This indicates that Co atoms are in the similar square-planar crystal field; the difference of crystal field splitting energy (corresponding to the distances between subpacks) comes from the difference of ligands.[39,40] Furthermore, considering that the Co-C coordination cannot be unambiguously distinguished from the Co-N coordination by EXAFS analysis, DFT calculations were employed to check the stability of various $CoN_{4-x}C_x$ moieties in graphene lattices ($CoN_{4-x}C_x$/G, X= 0, 1, 2, 3 and 4) by comparing the formation energies (see calculation details in the section of Methods). The calculation results and structural schematics are given in Figure 3c; it is obvious that $Co\text{-}N_4$/G moiety is much more energetic favorable than other $CoN_{4-x}C_x$/G (X= 1, 2, 3 and 4) compounds. In addition, the simulated Co K-edge XANES spectrum based on the structure model of a square-planar $Co\text{-}N_4$ doped graphene ($Co\text{-}N_4$/G) generated by DFT calculations is given in Figure 3d, in which excellent agreement is obtained

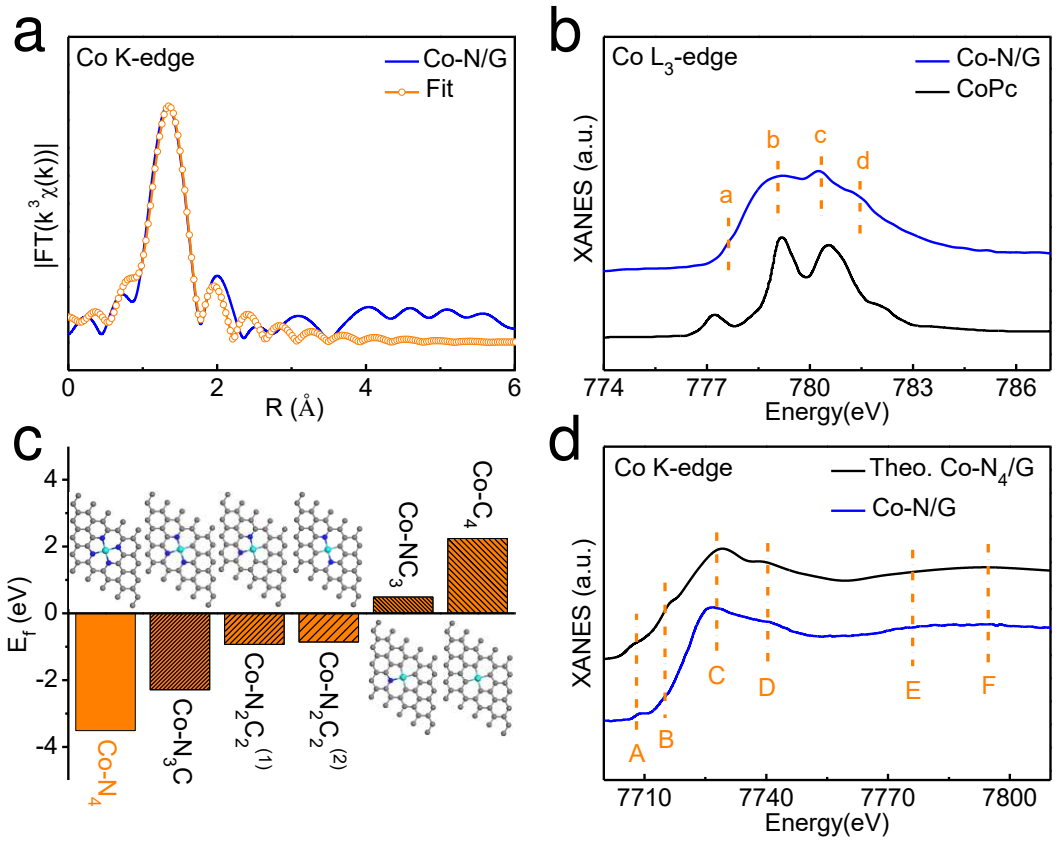

Figure 3. a) Co K-edge EXAFS fitting curves of Co-N/G nanosheets in *R*-space. b) Co L_3-edge XANES spectra for Co-N/G and CoPc reference. c) DFT-calculated formation energies of various Co-$N_{4-x}C_x$ moieties in graphene lattices (Co-$N_{4-x}C_x$/G, X= 0, 1, 2, 3 and 4), together with the structural schematics. The cyan, blue, and black gray spheres represent Co, N, and C atoms, respectively. d) Comparison of the experimental Co K-edge XANES spectrum of Co-N/G nanosheets and the simulated one based on a model of Co-N_4/G.

between the theoretical and experimental XANES spectra. All of the above experimental and theoretical results lead us to conclude that the square-planar Co-N_4 moieties is the most possible structure for Co atoms in the Co-N/G nanosheets**.**

Room-temperature ferromagnetism of graphene activated by the Co-N_4 moieties. Next, to clarify the effect of the Co-N_4 moieties on the magnetic properties of graphene nanosheets, we measured the magnetization curves ($M-H$) as a function of the applied magnetic field H (Figure 4a) at 300 K for pristine graphene and Co-N/G nanosheets. The well-defined hysteresis loop indicates the room-temperature ferromagnetic

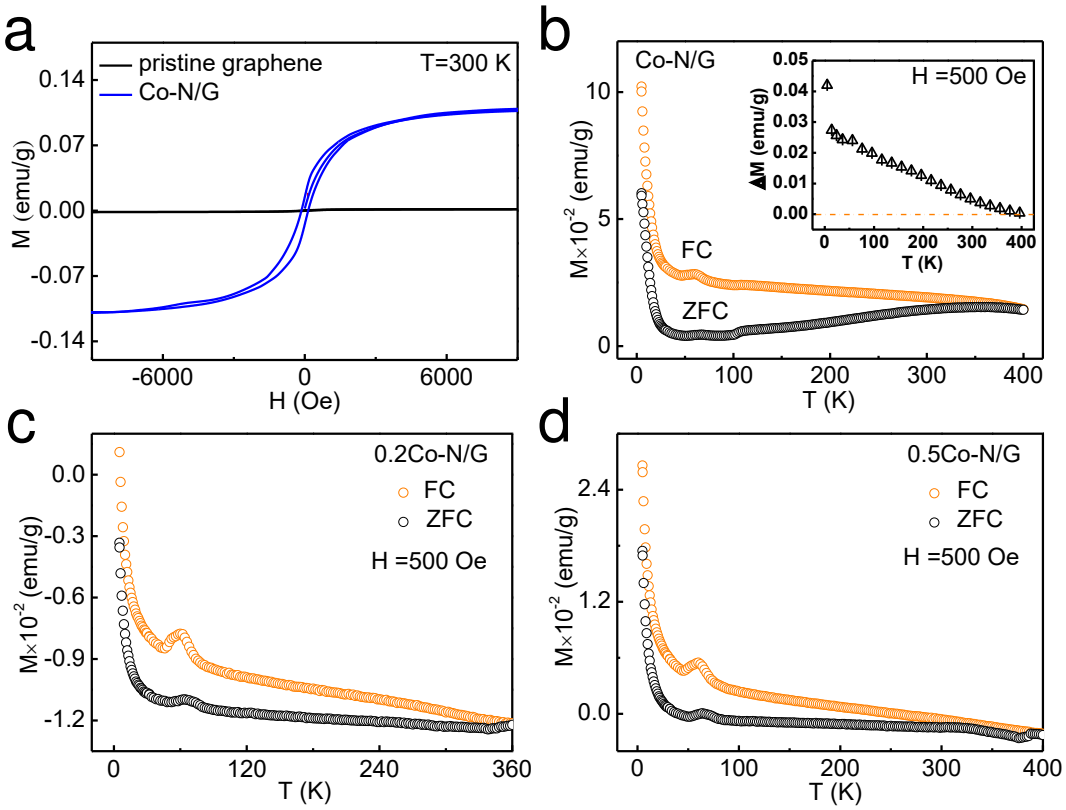

Figure 4. a) Magnetization vs magnetic field ($M-H$) curves for pristine graphene and Co-N/G nanosheets. b) Temperature dependence of FC and ZFC magnetization (M-T) curves for Co-N/G nanosheets. Inset: the magnetization difference (ΔM) between FC and ZFC curves (M_{FC}-M_{ZFC}) of Co-N/G nanosheets. c-d) Temperature dependence of FC and ZFC magnetization ($M-T$) curves for 0.2Co-N/G (c) and 0.5Co-N/G (d) nanosheets.

behavior of Co-N/G nanosheets with saturation magnetization and coercivity of about 0.11 emu/g and 142 Oe, respectively, different from the non-ferromagnetic properties of pristine graphene. In addition, temperature-dependent_magnetization curves ($M-T$) for Co-N/G nanosheets are given in Figure 4b under field-cooling (FC) and zero-field-cooling (ZFC) modes at an applied field of 500 Oe; it is clear that the Co-N/G nanosheets have a T_C of around 400 K. The magnetization difference (ΔM) between FC and ZFC curves (M_{FC}-M_{ZFC}) in the inset shows a decreasing trend but still perfectly positive in the whole temperature range. Hence, the possibility of spin glass effects and superparamagnetism can be exclued in the Co-N/G nanosheets.[24,41] A cusp at about 65 K in Figure 4b can be attributed to molecular oxygen on the surface as previously reported.[42,43,44] The corresponding $M-T$ curves for 0.2Co-N/G and 0.5Co-N/G under

an applied field of 500 Oe are also depicted in Figure 4c-d. It is obvious that magnetic moments take more negative values for 0.2Co-N/G (Figure 4c) and 0.5Co-N/G (Figure 4d) nanosheets, different from the distinct positive values over the entire temperature range for Co-N/G (Figure 4b), indicating the diamagnetic contribution from graphene is dominant at lower Co doping contents. All the samples exhibit thermo-magnetic irreversibility (a bifurcation in the FC and ZFC curves) at temperatures above 300 K. Furthermore, in order to visually show the change of magnetism with Co contents in doped graphene nanosheets, we extracted magnetic signals from the $M-H$ curves for all the samples and plotted them against the Co contents in Figure S7a. Obviously, the saturation magnetization for as-synthesized samples is enhanced when the Co content increases from 0.2× to 1.0× Co. At the content of 3.0× Co, according to the above characterization analysis, the ferromagnetism is not intrinsic and partly comes from the contribution of Co-based nanoparicles or/and clusters. At the temperature of 5 K, the $M-H$ curves for Co-N/G nanosheets exhibit similar ferromagnetism with higher saturation magnetization of about 0.73 emu/g (Figure S7b). If there is ferromagnetism derived from Co metal clusters, by comparing the magnetic moment of samples measured at 5 K (~0.4 μ_B/Co) with that of Co metal (1.7 μ_B/Co), we can estimate about 24% of the total doped Co atoms are in the form of clusters. Such a content of Co clusters should be easily detected by TEM and XANES,[45] which is however contrary to the experimental observations (Figure 1c and 1f). Meanwhile, the T_C of Co-N/G at about 400 K is much lower than that of Co metal clusters. In addition, we treated intrinsic non-magnetic Al_2O_3 powder under the same experimental and magnetic characterization conditions as for the Co-N/G nanosheets. No ferromagnetism was observed, which helps rule out the possibility of unintentional introduction of magnetic impurities during the experimental process. Hence, we can draw a safe conclusion on the intrinsic ferromagnetism in the Co-N_4 moiety doped graphene nanosheets.

Origin of the ferromagnetism of Co-N/C nanosheets. To obtain in-depth understanding on the origin of the room-temperature ferromagnetic coupling in Co-N/G nanosheets, spin-polarize density functional theory (DFT) calculations were performed

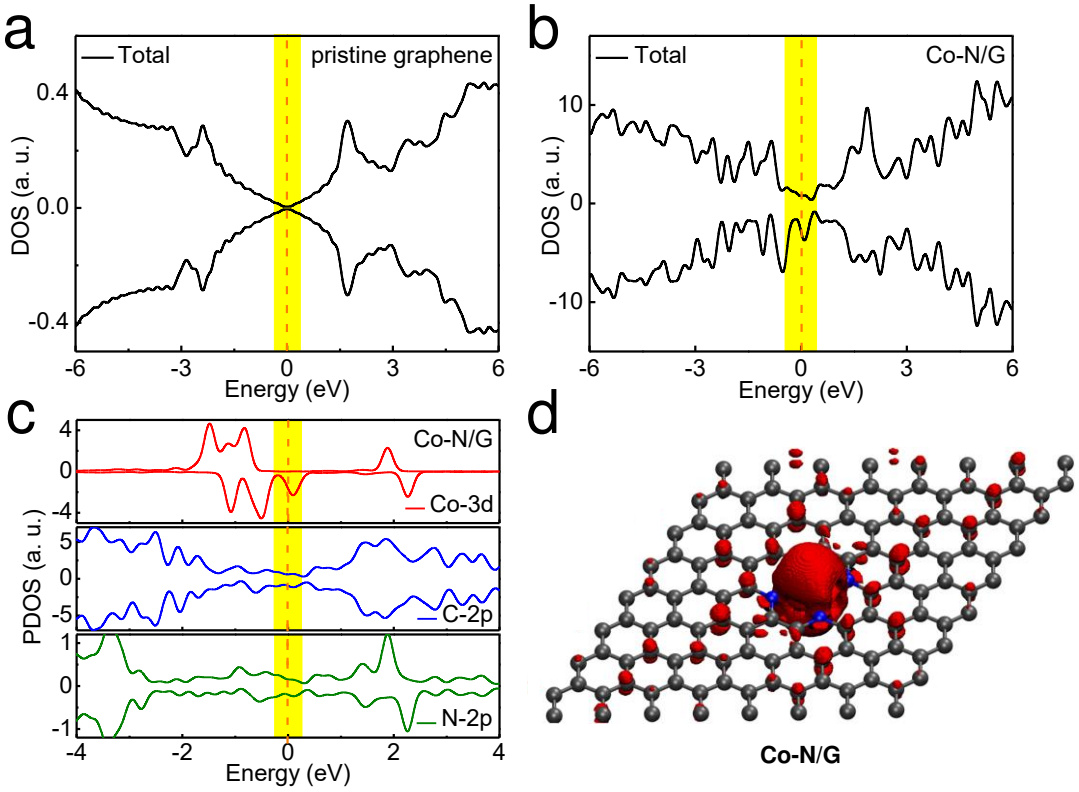

Figure 5. DFT calculated TDOS for a) pristine graphene and b) Co-N/G nanosheets. c) DFT calculated PDOS for Co-N/G nanosheets. d) Spatial distribution of spin density ($\rho\uparrow - \rho\downarrow$) for a 8×8×1 hexagonal graphene supercell with one doped square-planar Co-N_4 structure.

(see calculation details in the section of Methods). The total densities of states (TDOS), projected densities of states (PDOS) and spatial distribution of spin density are presented in Figure 5a-d, respectively. For reference, Figure 5a shows the TDOS of pristine graphene, which has no spin polarization and is semi-metallic with Dirac cone at the Fermi level (corresponding to E= 0 eV in the DOS).[46,47] In contrast, the TDOS of Co-N/G nanosheets (Figure 5b) exhibits significant spin polarization around the Fermi level, which is a typical indication for the intrinsic Stoner ferromagnetic coupling.[48,49,50] And according to the Stoner criterion,[51,52] high DOS of Co-N/G nanosheeets at the Fermi level ensure the ferromagnetic coupling at relative high temperature. The PDOS in Figure 5c further reveals the intense hybridization between the Co 3*d*, N 2*p* and C 2*p* electronic bands. The hybridization introduces spin polarization into the delocalized 2*p* bands of C and N atoms that contribute to the π bonds of graphene, providing spin-polarized itinerant electrons for the Stoner ferromagnetism.[50,53] In addition, according

to the spatial distribution of spin density (Figure 5d), there is a long-range ferromagnetic coupling between the local magnetic moment of Co, N and C atoms. And it is clear that the spin-polarized electrons in the graphene matrix are mainly the p_z electrons with high non-locality, further supporting the Stoner ferromagnetism maintained by spin-polarized itinerant electrons. Since the hybridization between the Co-3*d*, N-2*p* and C-2*p* electronic bands is essential for the Stoner ferromagnetic coupling in Co-N/G nanosheets, the strong room-temperature ferromagnetism originates from the chemical bonding that embed Co atoms into the graphene lattices. Hence the DFT simulations lead to the conclusion that the Co-N_4 moieties are responsible for the observed room-temperature ferromagnetism in the as-synthesized Co-N/G nanosheets. Moreover, it is worthy of note that the Co-N/G nanosheets have greatly improved performance of spin-polarized current because only one spin channel crosses the Fermi level.[31]

Discussion

In summary, we have explored the possibility of achieving stable room-temperature ferromagnetic ordering in graphene by embedding single magnetic TM atoms in the lattices through the strong chemical bonds in the TM-N_x moieties. A simple and controllable impregnation-pyrolysis process was employed to synthesize the Co-N-graphene system. Comprehensive structural characterizations confirm the existence of square-planar Co-N_4 moieties in the graphene lattices at the content of 0.4 at. % (for Co-N/G nanosheets), which displays unprecedented stable ferromagnetic ordering with T_C up to ~400 K and saturation magnetization of 0.11 emu/g (300 K). No Co-related second phase that may induce extrinsic ferromagnetism is observed. On the one hand, Co-N_4 moieties avoid the loss of Co atoms from the graphene lattices, thus providing a strong local magnetic moment; on the other hand, DFT calculation reveals that the room-temperature long-range ferromagnetic coupling originates from the hybridization between the Co 3*d* and C, N 2*p* orbitals through the Stoner ferromagnetism. This work developed stable room-temperature graphene magnets, which will pave the way towards practical graphene-based spintronic applications.

Methods

Synthesis of Co-N/G and N/G nanosheets. Co-N/G nanosheets were synthesized through a two-step impregnation-pyrolysis procedure. In the typical procedure, graphene oxide (GO) was firstly prepared by oxidation of powdered flake graphite following a modified Hummers' method.[54] Then, 50 μl of $CoCl_2 \cdot 6H_2O$ solution (3 mg ml^{-1}) and 15 μl of H_2O_2 solution (30%) were added dropwise into 10 ml of GO suspension (2 mg ml^{-1}) and the mixture was sonicated for 1 h. The obtained suspension was transferred into a stainless steel autoclave and maintained at 180 °C for 6 h, forming a hydrogel. After freeze drying, the Co^{2+}-containing gel was heated in the center of a quartz tube furnace at 900 °C for 1 h under gas flows of 100 sccm Ar and 50 sccm NH_3 to obtain Co-N/G. For comparison, the N/G nanosheets were prepared with the same procedure with no addition of $CoCl_2 \cdot 6H_2O$.

Synthesis of 0.2Co-N/G , 0.5Co-N/G and 3Co-N/G nanosheets. 0.2Co-N/G, 0.5Co-N/G and 3Co-N/G nanosheets were synthesized with a similar procedure to Co-N/G except for 0.2×, 0.5× and 3× Co precursors during preparation, respectively.

DFT calculation details. The spin-polarized density functional theory (DFT) calculations were performed with Quantum Espresso software package[55,56] and some calculation results were visualized with VMD software.[57] The electron exchange-correlation was processed within the framework of generalized gradient approximation (GGA) in the Perdew-Burke-Ernzerhof (PBE) parametrization. The electron-ion interaction was described using the projected augmented wave (PAW) method. The kinetic energy cutoffs of the plane wave and electron density were 80 and 500 Ry. The long-range van der Waals interaction was considered with the DFT-D3 scheme.[58] A 6×6×1 K-grid was used for sampling in the Brillouin zone. Energy convergence of 1.0 meV/atom was ensured during the self-consistent field calculations. And convergence criteria for the atomic forces was 0.05 eV/Å.

The Co embedded nitrogen-doped graphene nanosheets were modeled based on an 8×8×1 hexagonal supercell of graphene. Six adjacent carbon atoms were replaced with

Co-N_4 to form the Co-N/G structure. A vacuum layer of 15 Å was placed along the z direction to prevent the interlayer interaction.

The formation energies of Co-N_xC_{4-x} moieties in graphene were calculated according to the following equation,

$$E_f = E_{[Co-N_xC_{4-x}]} + (2+x)\mu_C - 64\mu_C - x\mu_N - E_{[Co(g)]}$$

where $E_{[Co-N_xC_{4-x}]}$ is the total energy of an 8×8×1 graphene supercell with a Co-N_xC_{4-x} moiety; μ_C and μ_N are the chemical potentials of C and N, defined as the total energy per atom in graphene and nitrogen molecules; $E_{[Co(g)]}$ is the total energy of an isolated Co atoms.

Data availability

The data that support the findings of this study are available from the corresponding authors upon reasonable request.

References

1. Li D, Kaner RB. Graphene-based materials. *Science* **320**, 1170-1171 (2008).
2. Stankovich S*, et al.* Graphene-based composite materials. *Nature* **442**, 282-286 (2006).
3. Stoller MD, Park S, Zhu Y, An J, Ruoff RS. Graphene-based ultracapacitors. *Nano Lett.* **8**, 3498-3502 (2008).
4. Lee C, Wei X, Kysar JW, Hone J. Measurement of the elastic properties and intrinsic strength of monolayer graphene. *Science* **321**, 385-388 (2008).
5. Novoselov KS*, et al.* Two-dimensional gas of massless dirac fermions in graphene. *Nature* **438**, 197-200 (2005).
6. Banszerus L*, et al.* Ultrahigh-mobility graphene devices from chemical vapor deposition on reusable copper. *Sci. Adv.* **1**, e1500222 (2015).
7. Balandin AA*, et al.* Superior thermal conductivity of single-layer graphene. *Nano Lett.* **8**, 902-907 (2008).
8. Vicarelli L*, et al.* Graphene field-effect transistors as room-temperature terahertz detectors. *Nat. Mater.* **11**, 865-871 (2012).
9. Liu Y, Dong X, Chen P. Biological and chemical sensors based on graphene materials. *Chem. Soc. Rev.* **41**, 2283-2307 (2012).
10. Antolini E. Graphene as a new carbon support for low-temperature fuel cell catalysts. *Appl. Catal. B-Environ.* **123**, 52-68 (2012).
11. Tombros N, Jozsa C, Popinciuc M, Jonkman HT, Van Wees BJ. Electronic spin

transport and spin precession in single graphene layers at room temperature. *Nature* **448**, 571-574 (2007).
12. Georgakilas V, Perman JA, Tucek J, Zboril R. Broad family of carbon nanoallotropes: classification, chemistry, and applications of fullerenes, carbon dots, nanotubes, graphene, nanodiamonds, and combined superstructures. *Chem. Rev.* **115**, 4744-4822 (2015).
13. Sepioni M*, et al.* Limits on intrinsic magnetism in graphene. *Phys. Rev. Lett.* **105**, 207205 (2010).
14. Tuček J*, et al.* Sulfur doping induces strong ferromagnetic ordering in graphene: effect of concentration and substitution mechanism. *Adv. Mater.* **28**, 5045-5053 (2016).
15. Palacios JJ, Fernández-Rossier J, Brey L. Vacancy-induced magnetism in graphene and graphene ribbons. *Phys. Rev. B* **77**, 195428 (2008)
16. Tuček J*, et al.* Room temperature organic magnets derived from sp^3 functionalized graphene. *Nat. Commun.* **8**, 14525 (2017).
17. Błoński P*, et al.* Doping with graphitic nitrogen triggers ferromagnetism in graphene. *J. Am. Chem. Soc.* **139**, 3171-3180 (2017).
18. González-Herrero H*, et al.* Atomic-scale control of graphene magnetism by using hydrogen atoms. *Science* **352**, 437-441 (2016).
19. Magda GZ*, et al.* Room-temperature magnetic order on zigzag edges of narrow graphene nanoribbons. *Nature* **514**, 608-611 (2014).
20. Ito Y*, et al.* Tuning the magnetic properties of carbon by nitrogen doping of its graphene domains. *J. Am. Chem. Soc.* **137**, 7678-7685 (2015).
21. Nair R*, et al.* Spin-half paramagnetism in graphene induced by point defects. *Nat. Phys.* **8**, 199-202 (2012).
22. Liu Y*, et al.* Elemental superdoping of graphene and carbon nanotubes. *Nat. Commun.* **7**, 10921 (2016).
23. Ahmed S*, et al.* Magnetic properties of Co doped WSe_2 by implantation. *J. Alloy. Compd.* **731**, 25-31 (2018).
24. Duan H*, et al.* Beating the exclusion rule against the coexistence of robust luminescence and ferromagnetism in chalcogenide monolayers. *Nat. Commun.* **10**, 1584 (2019).
25. Matsui D, Prylutskyy Y, Matzui L, Zakharenko M, Le Normand F, Derory A. Magnetic properties of cobalt-carbon nanocomposites. *Phys. Status. Solidi. C* **7**, 1264-1268 (2010).
26. Hota P, Akhtar A, Bhattacharya S, Miah M, Saha SK. Ferromagnetism in graphene due to charge transfer from atomic Co to graphene. *Appl. Phys. Lett.* **111**, 042402 (2017).
27. Wan X*, et al.* Fe–N–C electrocatalyst with dense active sites and efficient mass transport for high-performance proton exchange membrane fuel cells. *Nat. Catal.* **2**, 259-268 (2019).
28. Du Z*, et al.* Cobalt in nitrogen-doped graphene as single-atom catalyst for high-sulfur content lithium–sulfur batteries. *J. Am. Chem. Soc.* **141**, 3977-3985 (2019).

29. Sun T, *et al.* Single-atomic cobalt sites embedded in hierarchically ordered porous nitrogen-doped carbon as a superior bifunctional electrocatalyst. *P. Natl. Acad. Sci. USA* **115**, 12692-12697 (2018).
30. Chaban VV, Prezhdo OV. Nitrogen-nitrogen bonds undermine stability of N-doped graphene. *J. Am. Chem. Soc.* **137**, 11688-11694 (2015).
31. Sun YL, *et al.* Itinerant ferromagnetic half metallic cobalt-iron couples: promising bifunctional electrocatalysts for ORR and OER. *J. Mater. Chem. A* **7**, 27175-27185 (2019).
32. Zhu Y, *et al.* One-pot pyrolysis to N-doped graphene with high-density Pt single atomic sites as heterogeneous catalyst for alkene hydrosilylation. *Acs. Catal.* **8**, 10004-10011 (2018).
33. Yang Z, *et al.* Boosting oxygen reduction catalysis with Fe-N_4 sites decorated porous carbons toward fuel cells. *Acs. Catal.* **9**, 2158-2163 (2019).
34. Zhu C, *et al.* Hierarchically porous M–N–C (M= Co and Fe) single-atom electrocatalysts with robust MN_x active moieties enable enhanced ORR performance. *Adv. Energy Mater.* **8**, 1801956 (2018)
35. Zhao L, *et al.* Cascade anchoring strategy for general mass production of high-loading single-atomic metal-nitrogen catalysts. *Nat. Commun.* **10**, 1278 (2019).
36. Fei H, *et al.* Microwave-assisted rapid synthesis of graphene-supported single atomic metals. *Adv. Mater.* **30**, 1802146 (2018).
37. Zheng Y, *et al.* Hydrogen evolution by a metal-free electrocatalyst. *Nat. Commun.* **5**, 3783 (2014).
38. Alves MM, Dodelet J, Guay D, Ladouceur M, Tourillon G. Origin of the electrocatalytic properties for oxygen reduction of some heat-treated polyacrylonitrile and phthalocyanine cobalt compounds adsorbed on carbon black as probed by electrochemistry and X-ray absorption spectroscopy. *J. Phys. Chem.* **96**, 10898-10905 (1992).
39. Zhang T, *et al.* Conclusively addressing the CoPc electronic structure: a joint gas-phase and solid-state photoemission and absorption spectroscopy study. *J. Phys. Chem. C* **121**, 26372-26378 (2017).
40. Willey TM, *et al.* Electronic structure differences between H_2-, Fe-, Co-, and Cu-phthalocyanine highly oriented thin films observed using NEXAFS spectroscopy. *J. Chem. Phys.* **139**, 034701 (2013).
41. Hebard A, *et al.* Mining for high Tc ferromagnetism in ion-implanted dilute magnetic semiconductors. *J. Phys. D: Appl. Phys.* **37**, 511-517 (2004).
42. Felner I. Peculiar magnetic features and superconductivity in sulfur doped amorphous carbon. *Magnetochemistry* **2**, 34 (2016).
43. Prakash A, Misra S, Bahadur D. The role of reduced graphene oxide capping on defect induced ferromagnetism of ZnO nanorods. *Nanotechnology* **24**, 095705 (2013).
44. Ghosh B, Sardar M, Lahiri S, Banerjee S. Observation of superparamagnetism to flux closure behaviour in ZnO nanoparticle agglomerates. *J. Phys.: Condens. Matter* **24**, 366002 (2012).
45. Griffin KA, Pakhomov AB, Wang CM, Heald SM, Krishnan KM. Intrinsic

ferromagnetism in insulating cobalt doped anatase TiO_2. *Phys. Rev. Lett.* **94**, 157204 (2005).
46. Zheng J, Ren Z, Guo P, Fang L, Fan J. Diffusion of Li^+ ion on graphene: a DFT study. *Appl. Surf. Sci.* **258**, 1651-1655 (2011).
47. Majidi R, Karami A. Adsorption of formaldehyde on graphene and graphyne. *Physica E* **59**, 169-173 (2014).
48. Lee KW, Lee CE. Intrinsic impurity-band stoner ferromagnetism in $C_{60}H_n$. *Phys. Rev. Lett.* **106**, 166402 (2011).
49. Seo D-K, Kim S-H. Nature of Stoner condition for metallic ferromagnetism. *J. Comput. Chem.* **29**, 2172-2176 (2008).
50. Zoppellaro G*, et al.* Microwave energy drives "on-off-on" spin-switch behavior in nitrogen-doped graphene. *Adv. Mater.* **31**, 1902587 (2019).
51. Stoner EC. Collective electron ferromagnetism. *Proc. R. Soc. Lond.* **165**, 0372-0414 (1938).
52. Al Ma'Mari F*, et al.* Beating the Stoner criterion using molecular interfaces. *Nature* **524**, 69-U128 (2015).
53. Li Y, He J, Kong X, Kou SP. Vacancy-induced intrinsic magnetic impurity with quasilocalized spin moment in graphene. *Phys. Rev. B* **90**, 201406 (2014).
54. Hummers Jr WS, Offeman RE. Preparation of graphitic oxide. *J. Am. Chem. Soc.* **80**, 1339-1339 (1958).
55. Giannozzi P*, et al.* QUANTUM ESPRESSO: a modular and open-source software project for quantum simulations of materials. *J. Phys.: Condens. Matter* **21**, 395502 (2009).
56. Gonze X*, et al.* ABINIT: First-principles approach to material and nanosystem properties. *Comput. Phys. Commun.* **180**, 2582-2615 (2009).
57. Humphrey W, Dalke A, Schulten K. VMD: visual molecular dynamics. *J. Mol. Graph.* **14**, 33-38 (1996).
58. Grimme S, Ehrlich S, Goerigk L. Effect of the damping function in dispersion corrected density functional theory. *J. Comput. Chem.* **32**, 1456-1465 (2011).

Acknowledgements

This work was financially supported by the National Natural Science Foundation of China (Grants No. 11975234, 11775225 and U1632263), the Users with Excellence Program of Hefei Science Center CAS (2019HSC-UE002), the Innovative Program of Development Foundation of Hefei Center for Physical Science and Technology (Grant No. 2018CXFX011), the Postdoctoral Science Foundation of China (Grants No. 2019M662202), and partially carried out at the USTC Center for Micro and Nanoscale Research and Fabrication. The authors would like to thank BSRF, SSRF and NSRL for the synchrotron radiation beamtime.

Author contributions

The manuscript was written through contributions of all authors. All authors have given approval to the final version of the manuscript.

Competing interests

The authors declare no competing interests.

Additional information

Supplementary Information accompanies this paper is available at

Correspondence and requests for materials should be addressed to W.Y.

Table of Contents

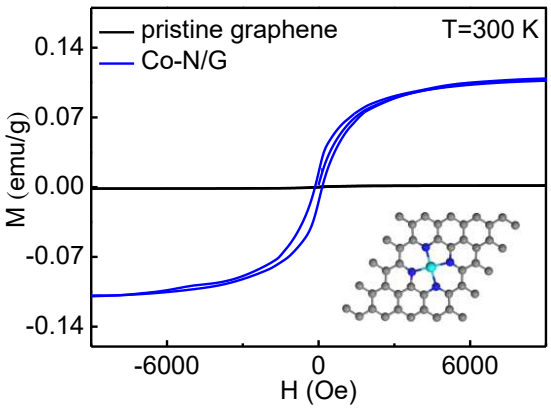

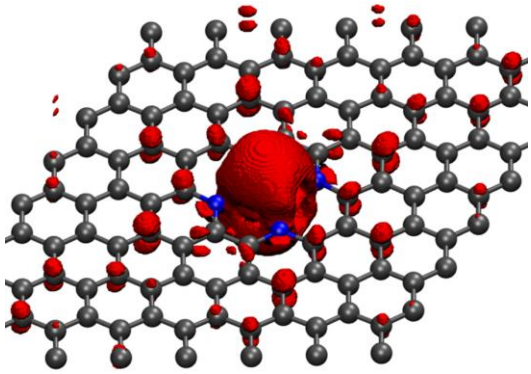

Co-N/G

Figures

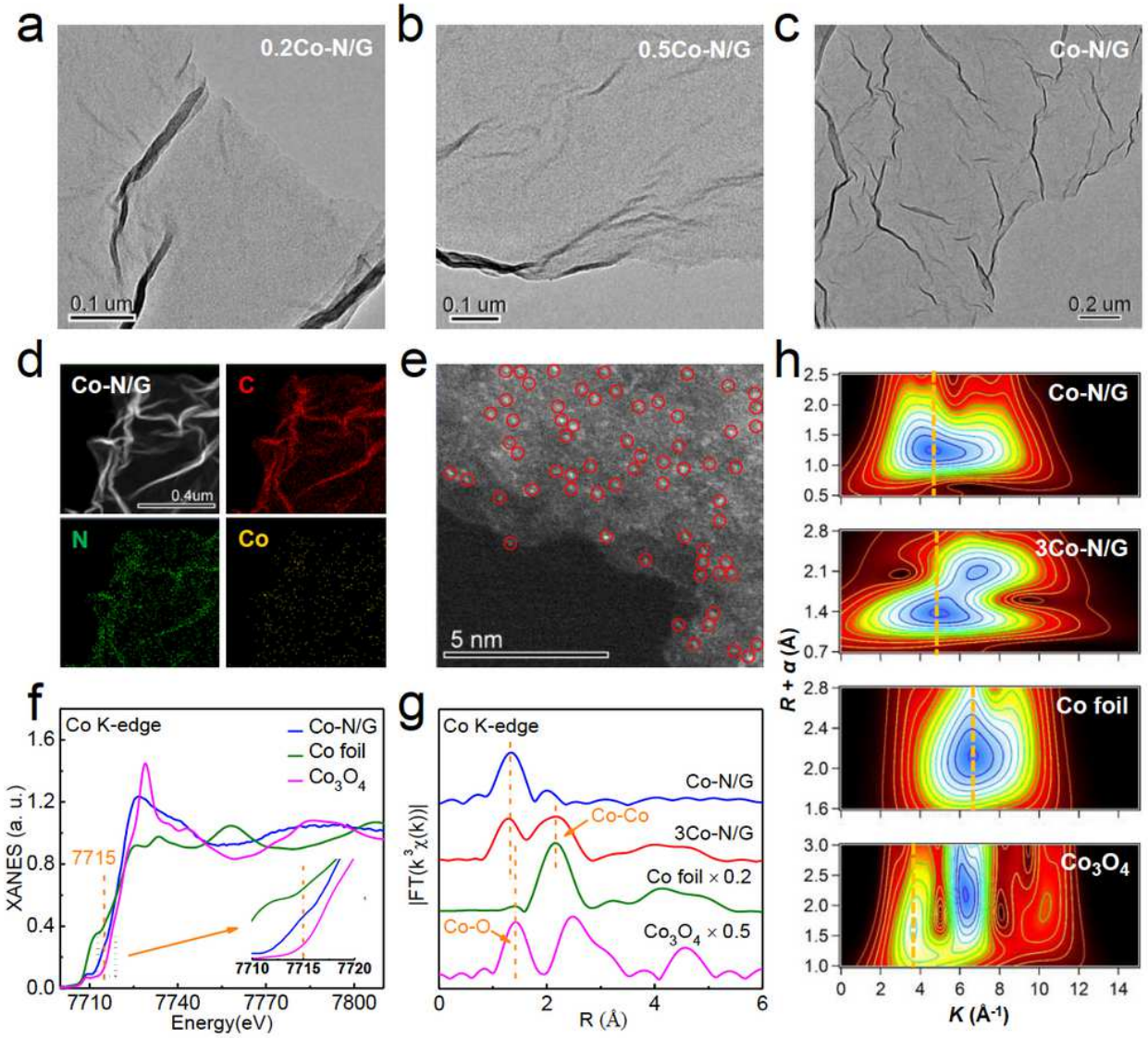

1

Figure 1

TEM images of a) 0.2Co-N/G , b) 0.5Co-N/G and c) Co-N/G samples . d) EDX elemental mapping and e) HAADF-STEM image of Co-N/G . f) Co K-edge XANES spectra for Co-N/G and reference samples. g) FT k3-weighted Co K-edge EXAFS spectra and h) WT analysis of EXAFS spectra for Co-N/G , 3 Co-N/G and reference samples.

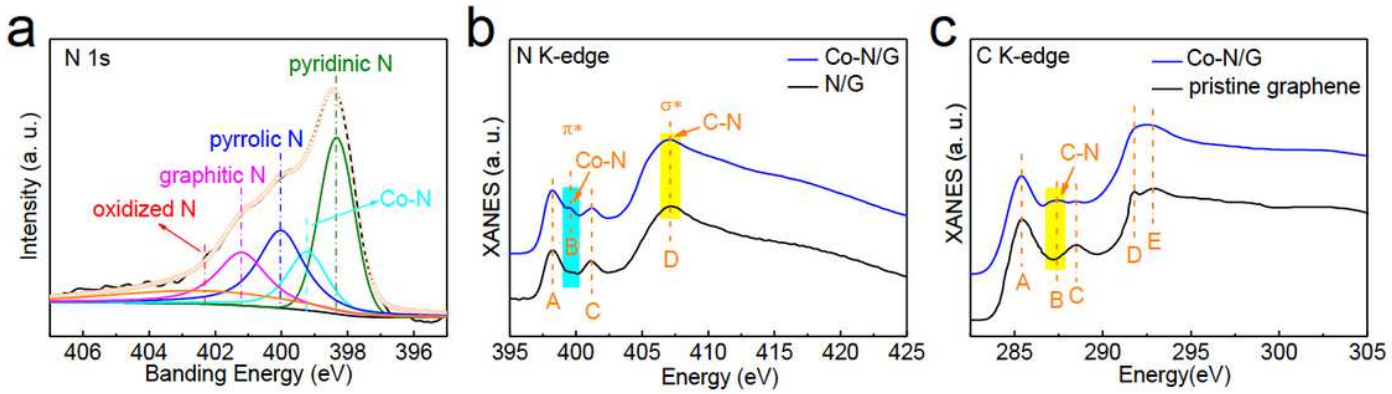

Figure 2

a) N 1s XPS spectrum of Co-N/G nanosheets. b) N K-edge XANES spectra of Co-N/G and N/G nanosheets. c) C K-edge XANES spectra of Co-N/G nanosheets and pristine graphene.

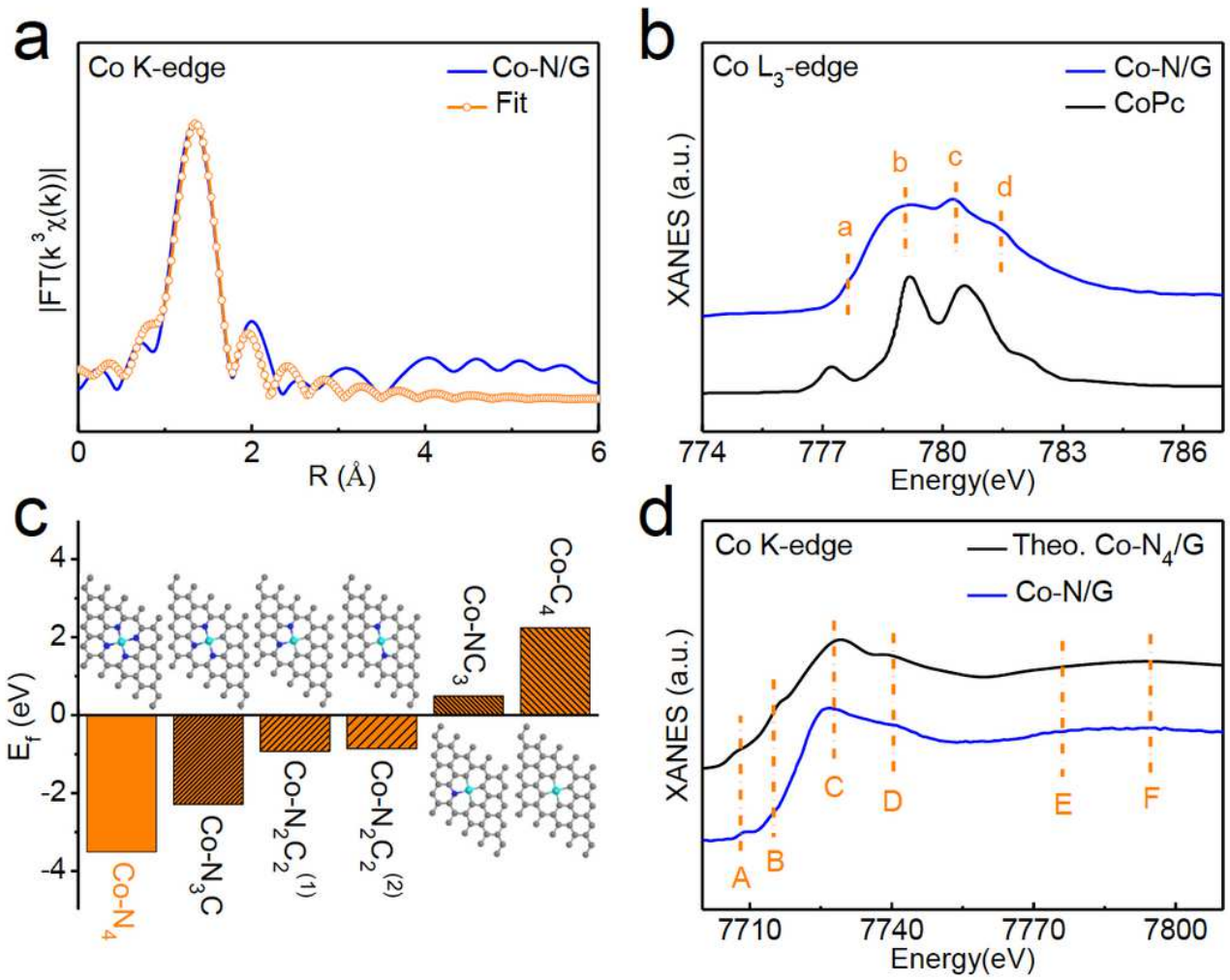

Figure 3

a) Co K-edge EXAFS fitting curves of Co-N/G nanosheets in R space. b) Co L3 edge XANES spectra for Co-N/G and CoPc reference. c) DFT-calculated formation energies of various Co-N4-xCx moieties in graphene lattices (Co-N4-xCx/G, X= 0, 1, 2, 3 and 4), together with the structural schematics. The cyan, blue, and black gray spheres represent Co, N, and C atoms, respectively. d) Comparison of the experimental Co K-edge XANES spectrum of Co-N/G nanosheets and the simulated one based on a model of Co-N4/G.

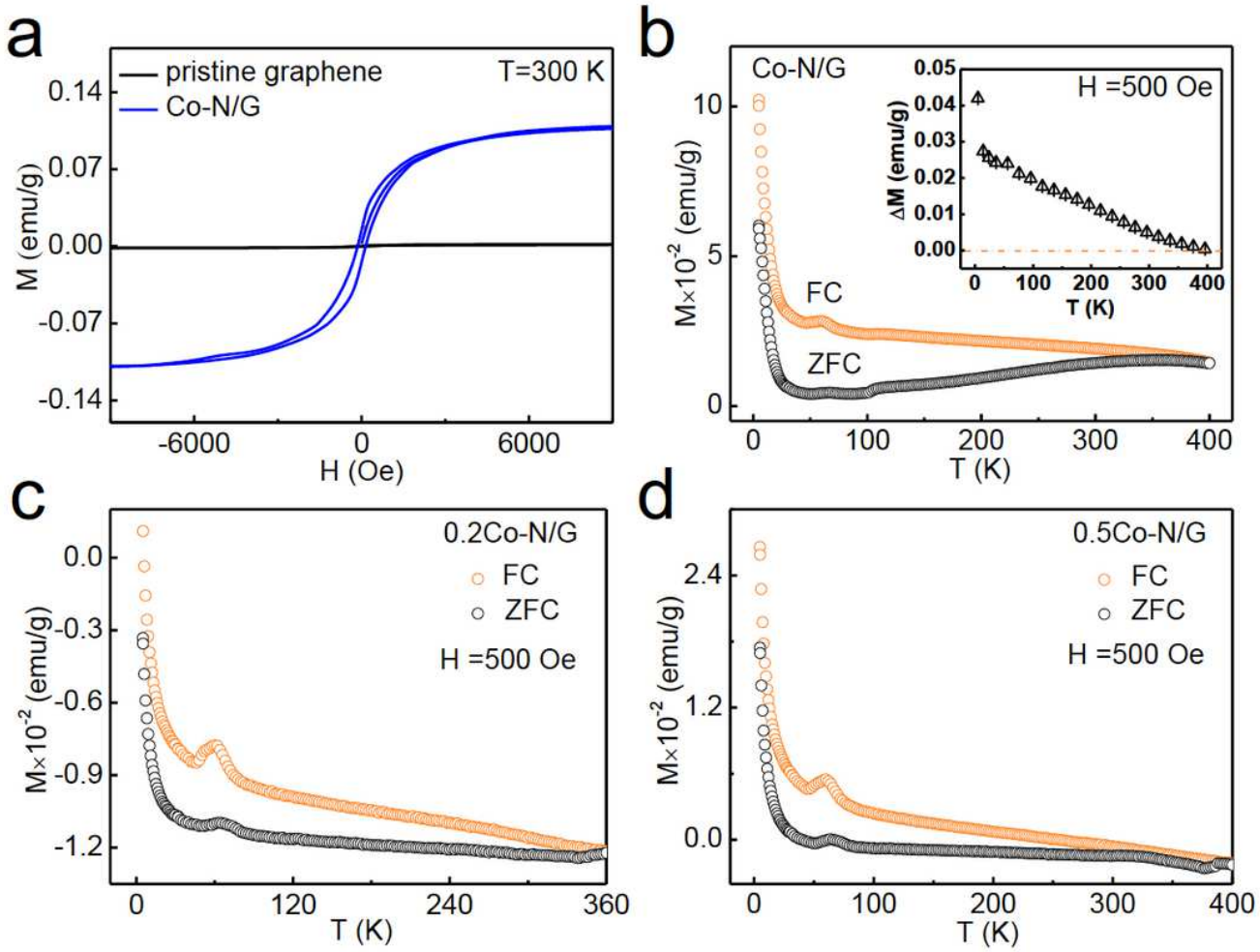

Figure 4

a) Magnetization vs magnetic field (M−H) curves for pristine graphene and Co-N/G nanosheets. b) Temperature dependence of FC and ZFC magnetization (M-T) curves for Co-N/G nanosheets. Inset: the magnetization difference (ΔM) between FC and ZFC curves (MFC-MZFC) of Co-N/G nanosheets. c-d) Temperature dependence of FC and ZFC magnetization (M−T) curves for 0.2Co-N/G c) and 0.5Co-N/G d) nanosheets.

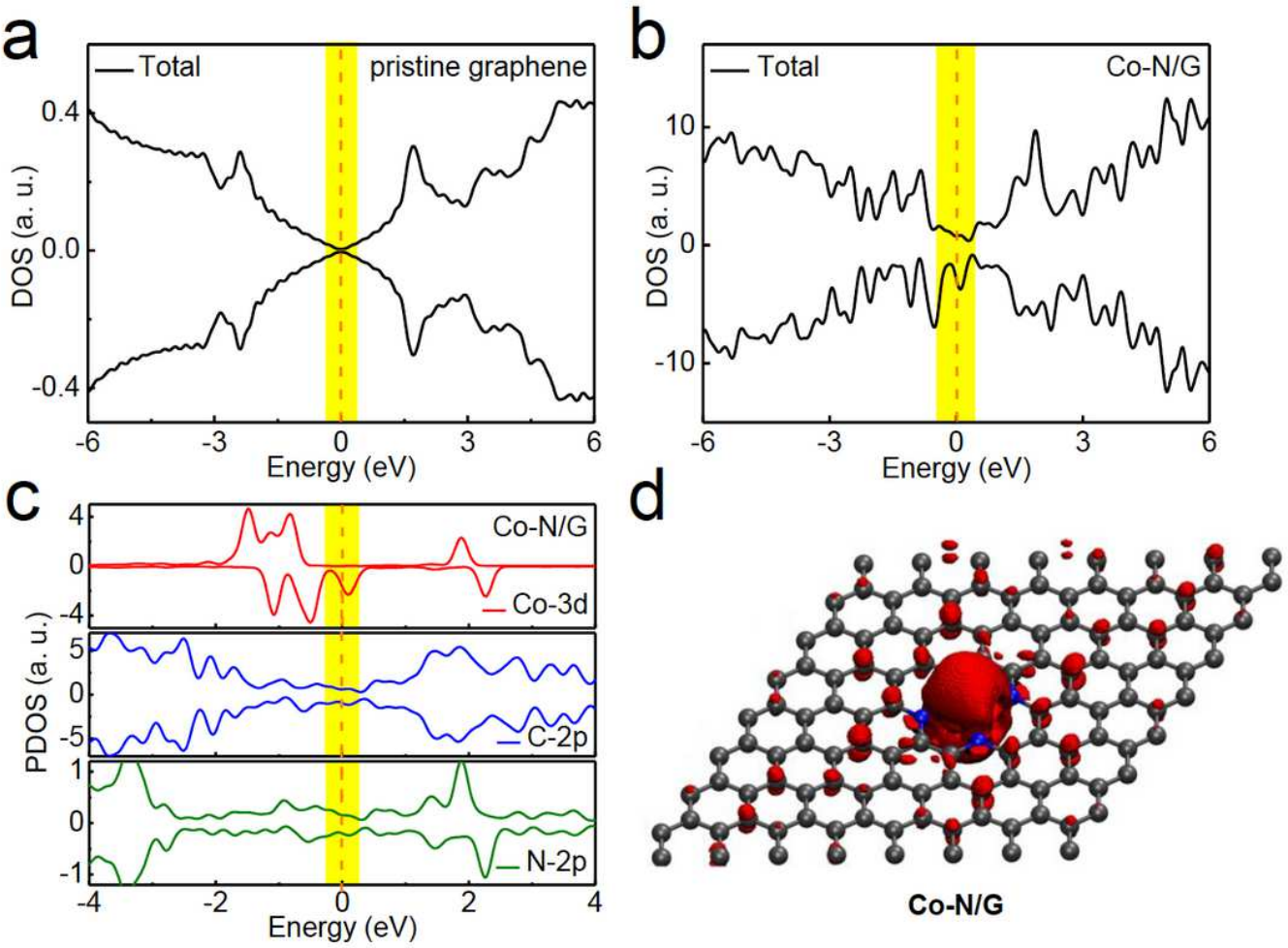

Figure 5

DFT calculated TDOS for a) pristine graphene and b) Co-N/G nanosheets. c) DFT calculated PDOS for Co-N/G nanosheets. d) Spatial distribution of spin density (ρ↑-ρ↓) for a 8×8×1 hexagonal graphene supercell with one doped square-planar Co-N4 structure.

Supplementary Files

This is a list of supplementary files associated with this preprint. Click to download.

- Roomtemperatureferromagnetismofgraphenesupportinginformation.pdf